Award number: 00HQGR0007

STUDY OF THE MOHO DEPTH AND CRUSTAL Vp/Vs VARIATION IN SOUTHERN CALIFORNIA FROM TELESEISMIC WAVEFORMS

Ta-liang Teng and Lupei Zhu
University of Southern California
Department of Earth Sciences, USC, Los Angeles, CA 90089-0740
email: lteng@terra.usc.edu; Tel: 213 740-5838; Fax: 213 740-8801

Program Element: II
Key Words: wave propagation, seismotectonics, strong ground motion

Research supported by the U.S. Geological Survey (USGS), Department of the Interior, under USGS award number 00HQGR0007. The views and conclusions contained in this document are those of the authors and should not be interpreted as necessarily representing the official policies, either expressed or implied, of the U.S. Government.

Award number: 00HQGR0007

STUDY OF THE MOHO DEPTH AND CRUSTAL Vp/Vs VARIATION IN SOUTHERN CALIFORNIA FROM TELESEISMIC WAVEFORMS

Ta-liang Teng and Lupei Zhu
University of Southern California
Department of Earth Sciences, USC, Los Angeles, CA 90089-0740
email: lteng@terra.usc.edu; Tel: 213 740-5838; Fax: 213 740-8801

Abstract

More than 54,000 high quality three-component waveform records from 817 large teleseismic earthquakes between 1993 and 2001 were collected and processed. From these waveforms we obtained 15,469 teleseismic receiver functions for 157 broadband seismic stations in southern California. We used an improved H-κ stacking algorithm to estimate crustal thickness and Vp/Vs ratio under each station from Moho P-to-S converted waves in receiver functions. The method first stacks all receiver functions with a move-out correction for different ray-parameters. This allows us to identify the Moho Ps phase and measure its time delay with respect to the direct P. We then stacked Moho multiple converted phases ($PpPs$ and $PsPs$+$PpSs$) predicted by the Ps delay and different crustal Vp/Vs ratio. The maximum stacking amplitude gives the "optimal" estimate of Vp/Vs ratio. Finally, the Ps delay and the crustal Vp/Vs ratio are converted to the crustal thickness. The results show that the average crustal thickness in southern California is about 30 km. Places such as the western Peninsular Range, the eastern Transverse Range, and west of Sierra Nevada Range have thicker crust, while regions of the Salton trough and offshore California Borderland have thinner crust. The crustal Vp/Vs ratio ranges from 1.64 to 1.87 with an average of 1.76. Amplitude variation of the Moho P-to-S converted wave indicates that crustal blocks west of the San Andreas Fault has smaller crustal/mantle velocity contrast than those east of the fault.

Non-Technical Abstract

More than 54,000 high quality three-component waveform records from 817 large teleseismic earthquakes between 1993 and 2001 were collected and processed. From these waveforms we obtained 15,469 teleseismic receiver functions for 157 broadband seismic stations in southern California. We used a stacking algorithm to estimate crustal thickness and Vp/Vs ratio under each station. The results show that the average crustal thickness in southern California is about 30 km. Places such as the western Peninsular Range, the eastern Transverse Range, and west of Sierra Nevada Range have thicker crust, while regions of the Salton trough and offshore California Borderland have thinner crust. The crustal Vp/Vs ratio ranges from 1.64 to 1.87 with an average of 1.76. Amplitude variation of the Moho P-to-S converted wave indicates that crustal blocks west of the San Andreas Fault has smaller crustal/mantle velocity contrast than those east of the fault.

1 Data Collection

During the two years of this project, we have collected and processed 54,486 three-component teleseismic P waveform records of 157 broadband stations in southern California. The stations include 136 Caltech-USGS-CDMG TriNet stations, 13 Anza array stations, and 7 temporary broadband stations in the 1994 Peninsular seismic recording experiment [*Ichinose et al.*, 1996]. Their locations are shown in Fig. 1. Average station spacing is about 50 km, close to the proposed USArray station spacing.

The waveforms were recorded from 817 earthquakes between January 1993 and September 2001 (Fig. 2). These earthquakes are all located beyond 25° in epicentral distance from the center of TriNet array and have magnitudes larger than 5.5. Large number of events in South America, western Pacific, Japan, and Aleutian-Alaska provides good coverages for these azimuths.

The data are processed according to the proposed research plan. Each seismogram was visually examined to make sure that it has good signal/noise ratio. The inspection was done by aligning all vertical component records from the same event on the P onset using a multi-channel cross-correlation technique. A graphics user interface program were written to allow us to chose correlation window and adjust the alignment interactively. This greatly reduces the time to inspect all waveform records. This process also produced very accurate first P arrival picks that will be used for a seismic tomograph study of the region in the future. Fig. 3 shows the P-wave station delays by averaging relative travel-time residuals for each station. Most of the positive delays can be explained by thick sedimentary basins in the Los Angeles Basin, the Imperial Valley, and the Ventura/San Fernando Valleys. We find several areas with large negative delays (west of Sierra-Nevada Range, Santa Monica Mountains and Eastern Transverse Range, and western Peninsular Range). Some of them might be related to the reported upper mantle high velocity anomalies [*Hadley and Kanamori*, 1977; *Humphreys and Clayton*, 1990; *Zhao et al.*, 1996].

2 H-κ stacking of receiver functions

We used an iterative time-domain deconvolution technique to compute receiver functions [*Kikuchi and Kanamori*, 1982; *Ligorria and Ammon*, 1999]. This deconvolution technique is very stable, especially at long periods and for noisy data. Causality in receiver function is also guaranteed in the deconvolution. We found that it yields better receiver functions than other techniques such as the spectrum division or the time-domain Wiener deconvolution. The deconvolution results were visually checked and bad traces were discarded. In total, we obtained 15,469 receiver functions.

We then stack receiver functions of each station using different crustal thickness (H) and Vp/Vs ratio (κ) to estimate the "optimal" H and κ under the station (for detail, see *Zhu and Kanamori* [2000]). We improved the H-κ stacking by separating it into two steps. We first only stack the primary converted phases for different H while fixing κ. The location of the maximum stacking amplitude gives the "optimal" crustal thickness for this κ. This thickness is converted back to the time delay of the Moho P-to-S converted wave (Ps). We find that this is a robust estimate of the Moho Ps time delay and it is essentially not

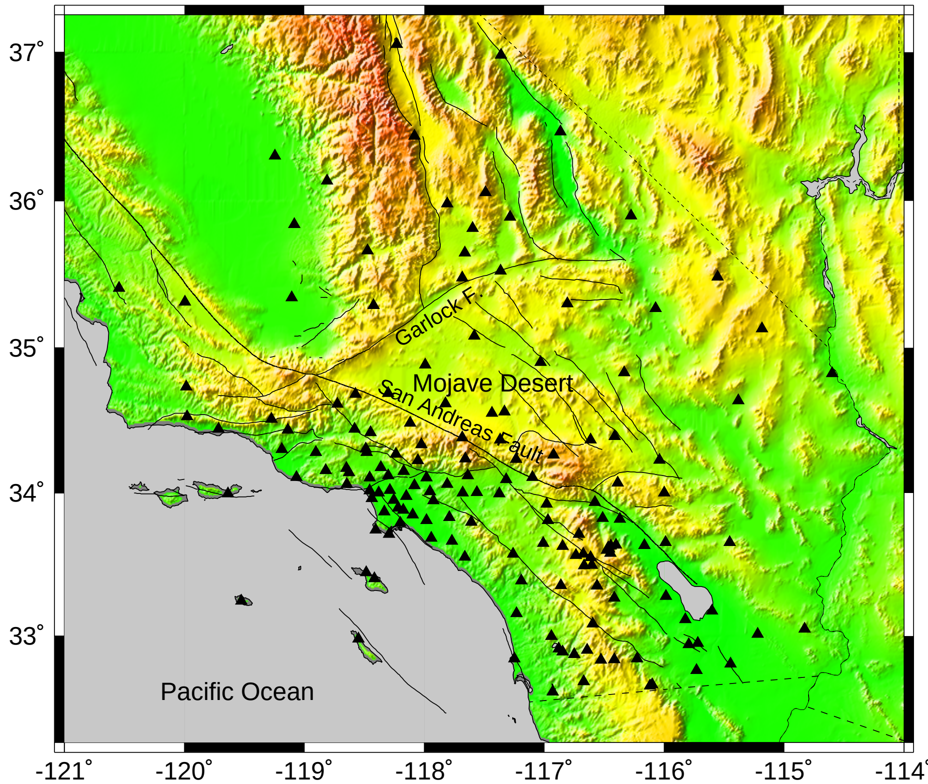

Figure 1: Station locations of broadband stations (triangles) used in the study.

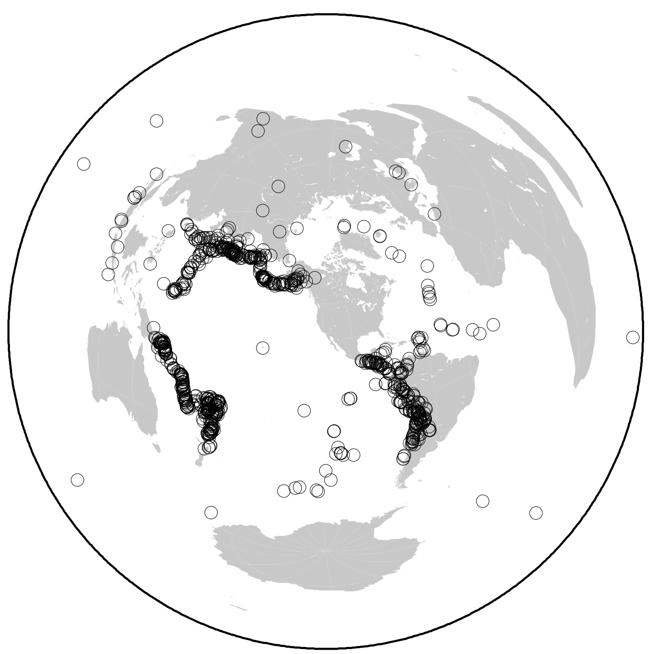

Figure 2: Equal-distance projection of the locations of 817 earthquakes used in this study with respect to the center of the TriNet array.

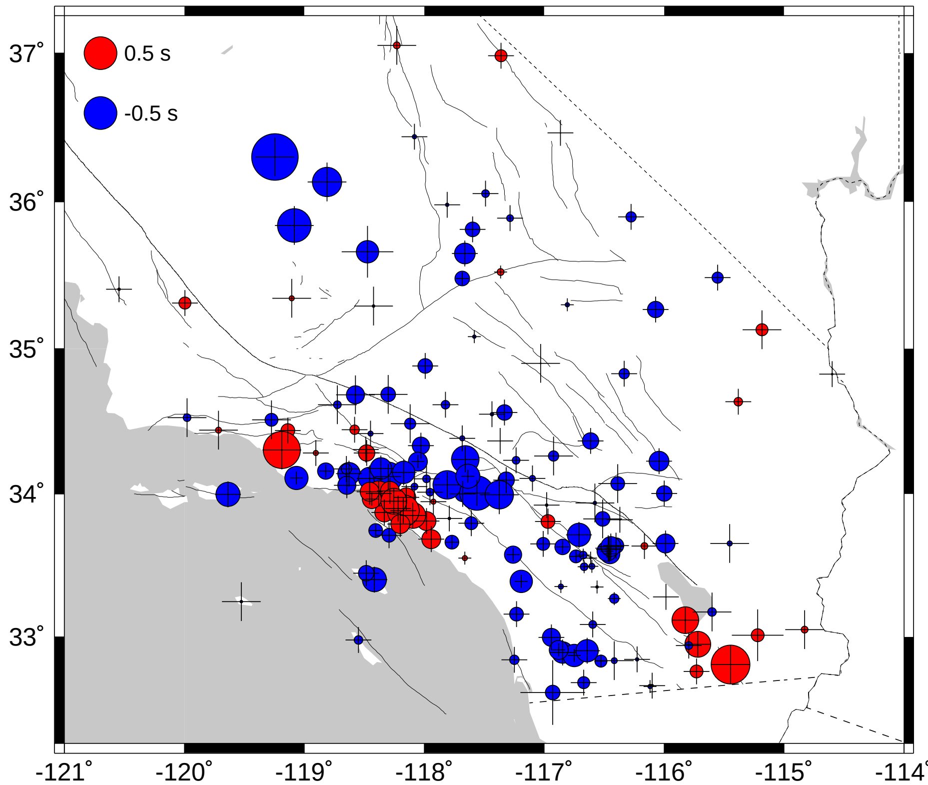

Figure 3: P wave station delays, red means later P arrival with respect to the IASPEI earth model. They have been corrected to the sea level using a P velocity of 5.5 km/s and a ray-parameter of 0.06 s/km. The size of the cross is proportional to standard deviation.

dependent on the assumed crustal Vp/Vs ratio. The next step is to stack multiple Moho converted phases ($PpPs$ and $PsPs + PpSs$) for different κ while requiring that κ and H satisfy the measured Ps delay constraint:

$$s(\kappa) = w_2 r(t_2) - w_3 r(t_3),$$

where $r(t)$ is the radial receiver function, t_2 and t_3 are the predicted $PpPs$, and $PsPs$+$PpSs$ arrival times corresponding to crustal thickness H and Vp/Vs ratio κ. We chose the weighting factors $w_2 = 0.7$ and $w_2 = 0.3$. The maximum of this κ-stacking gives the "optimal" crustal Vp/Vs ratio. Fig. 4 shows an example of stacking for station PAS.

3 Results

All the results are listed in Table 1. In total, we picked Moho P-to-S converted phases on 120 stations. The rest 37 stations, most of them are located on top of thick sedimentary basins, are too noisy for identifying the Moho Ps phase. Fig. 5 shows the Moho Ps delays with respect to the direct P arrivals and their amplitudes on the 120 stations. We found that in the Peninsular Range, the eastern Transverse Range, and west of Sierra Nevada Range, the Moho Ps delays are large while the delays are small for stations located in the

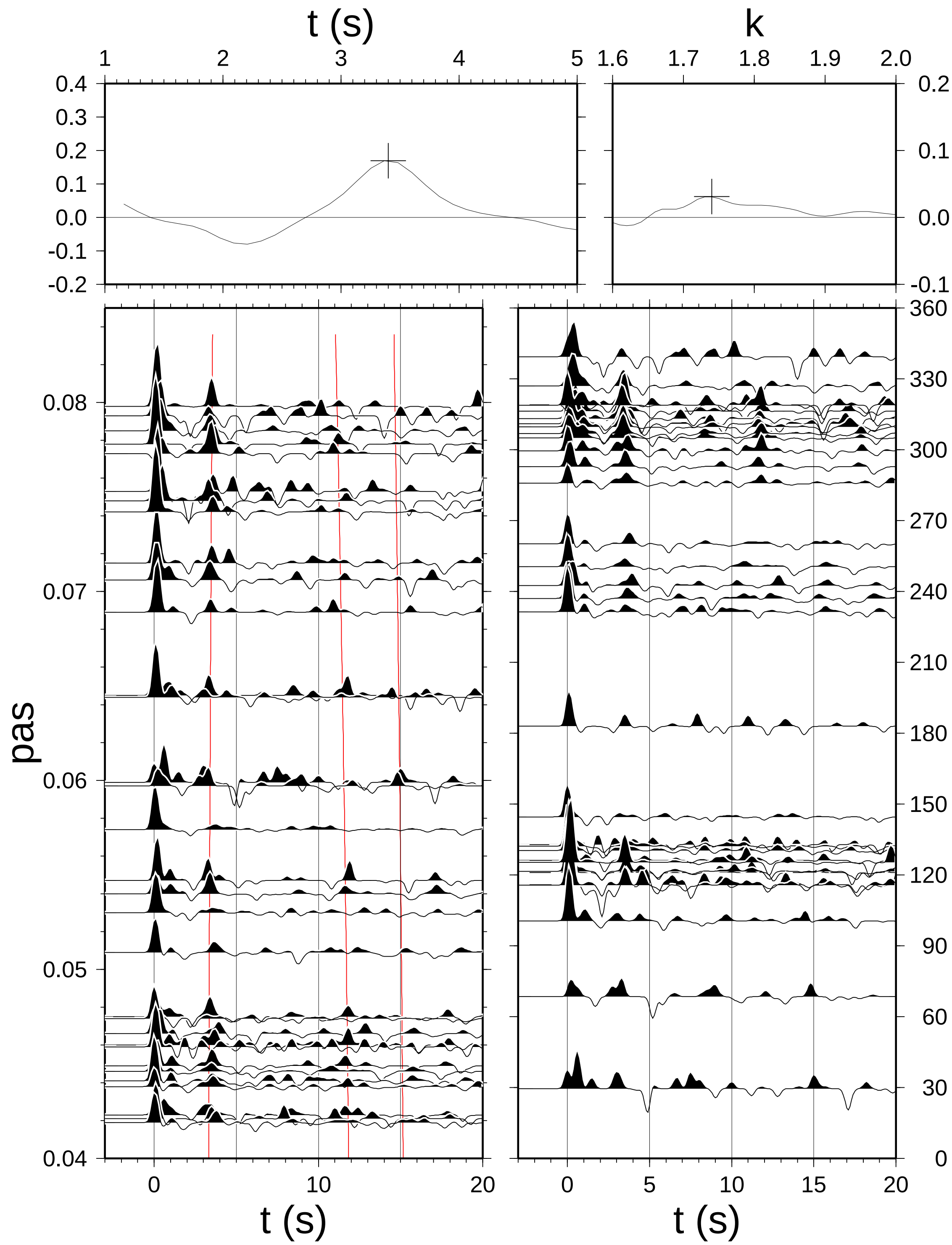

Figure 4: H and κ stacking of PAS receiver functions. Upper-left is stacking all receiver functions with move-out correction for different ray-parameters. The cross indicates the Moho Ps. Upper-right is a stacking of multiple Moho converted waves for different crustal Vp/Vs ratio κ. The maximum amplitude (cross) gives the "optimal" κ. The bottom shows receiver functions for different ray-parameters (left) and back-azimuths (right).

Salton Trough and offshore California Borderland. The Moho Ps delays for stations in the Mojave Desert are close to the average (4 s). To the first order, these reflect crustal thickness variation in the region. The amplitudes of Moho Ps also show systematical variation: in the Pacific side of the San Andreas Fault (SAF), the Moho P-to-S conversion amplitudes are smaller compared with the North American side of the fault (Fig. 5). This indicates that the velocity contrast across Moho in the Pacific side of SAF is smaller than in the North America side. SAF represents a major boundary that separates two kinds of crustal blocks.

Constraining crustal Vp/Vs ratio is more difficult. Out of the 120 stations, only 56 stations have stable Moho P-to-S conversion multiples to give significant peaks in the κ-stacking. The average Vp/Vs ratio for southern California crust is 1.76 from the 56 station measurements which range from 1.64 to 1.87 (Fig. 6). Three stations located offshore show consistent low Vp/Vs ratios. High Vp/Vs ratios are found for stations in Mesozoic mountain ranges.

Finally, the Moho Ps delays were converted into crustal thickness using the above crustal Vp/Vs ratios and a crustal P velocity of 6.3 km/s (Fig. 6). For stations that no Vp/Vs measurement is available, the average ratio of 1.76 is used. We found that the average Moho depth in southern Californian crust is 29.7 km. Moho depths under most stations are close to the average value. Crust is thin in the offshore California Borderland and the Salton Trough and thick in the western Peninsular Range, the eastern Transverse Range, and west of the Sierra-Nevada Range. No crustal root is found under the western and central Transverse Range.

4 Publications

1. L. Zhu and L. A. Rivera. A note on the dynamic and static displacements from a point source in multi-layered media. *Geophys. J. Int.*, in press, 2002.

2. Y. Ben-Zion and L. Zhu. Potency-magnitude scaling relations for southern California earthquakes with $1.0 < M_L < 7.0$. *Geophys. J. Int.*, in press, 2002.

3. L. Zhu. Summary of results of crustal structures using teleseismic waveforms from LARSE (abstract). *Eos Trans. AGU*, 82 (47):Fall Meeting Suppl., 2001.

4. L. Zhu. High resolution imaging of deep structure across plate boundary using seismic waves (abstract). In *Plate Boundary Observatory–Taiwan Workshop*, Taipei, Oct. 2001.

5. L. Zhu. Summary of results of crustal structures using teleseismic waveforms from LARSE (abstract). In *Annual SCEC Meeting*, Oxnard, CA, September 2001.

6. L. Zhu. High resolution imaging of crustal structure across the San Andreas Fault (abstract). In *SEG Summer Research Workshop*, Newport Beach, CA, July 2001.

7. L. Zhu. Preliminary results of crustal structure from the LARSE-II passive recording experiment using teleseismic P-to-S converted waves (abstract). In *97th Annual Meeting of Geol. Soc. Am. Cordilleran Section*, Universal City, CA, May 2001.

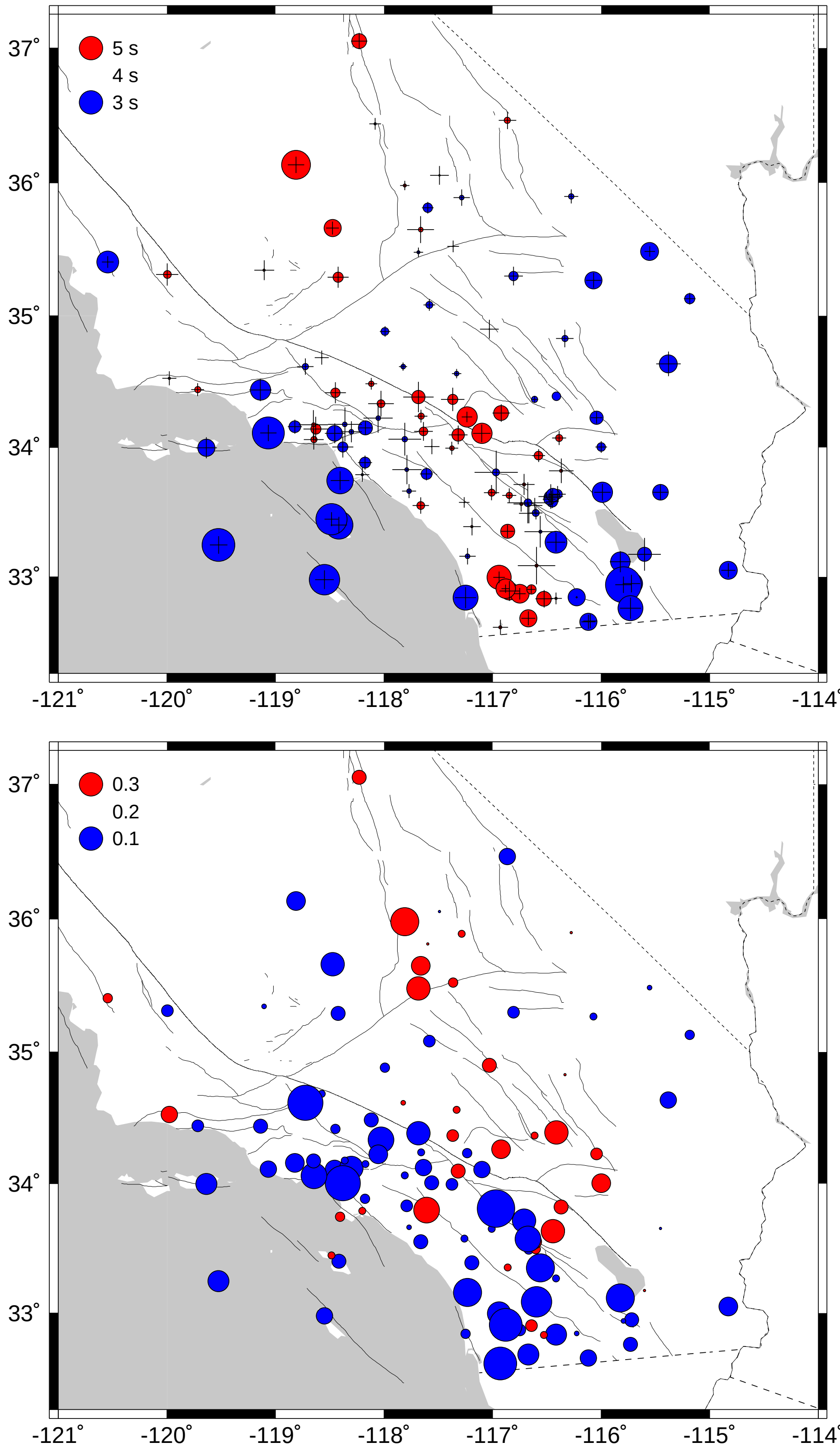

Figure 5: Moho Ps delays with respect to the first P arrival (upper, normalized to a ray-parameter of 0.06 s/km) and amplitudes (bottom).

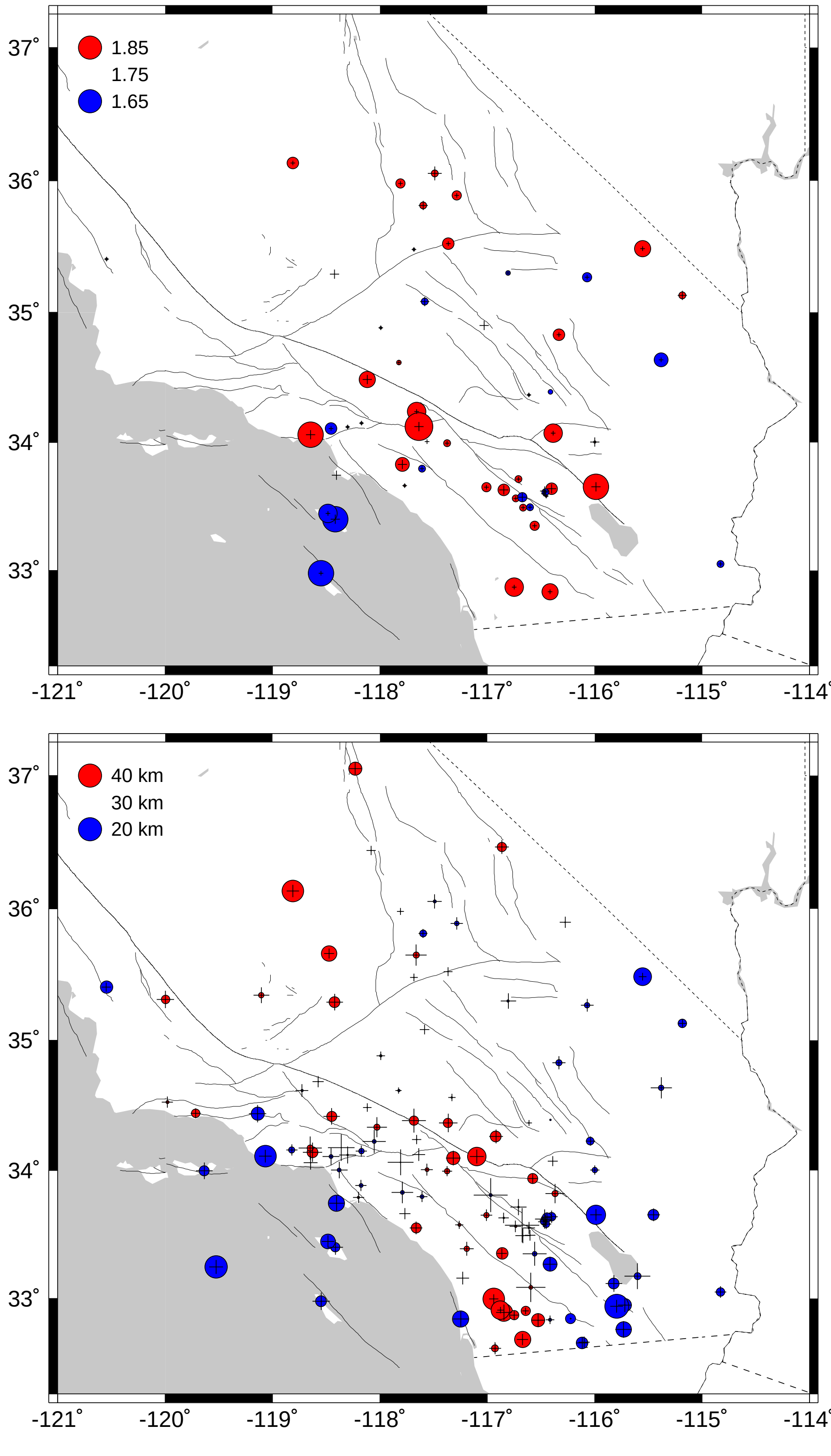

Figure 6: Crustal Vp/Vs ratio (upper) and Moho depth (bottom) from H-κ stacking. The size of the cross is proportional to the standard deviation.

8. L. Zhu and M. D. Kohler. Preliminary results of crustal structure from the LARSE-II passive recording experiment using teleseismic P-to-S converted waves (abstract). *Eos Trans. AGU*, 81:Fall Meeting Suppl., 2000.

5 Data availability

The estimated crustal thicknesses and Vp/Vs ratios of the 120 broadband stations in southern California are available via anonymous ftp to ftp.eas.slu.edu. The results are in plain text format named as /pub/lupei/sc2002.tbl. For detailed information, contact Lupei Zhu (email: lupei@eas.slu.edu, Tel: 314 977-3118).

References

Hadley, D., and H. Kanamori, Seismic structure of the Transverse Ranges, California, *Geol. Soc. Am. Bull.*, *88*, 1469–1478, 1977.

Humphreys, E. D., and R. W. Clayton, Tomographic image of the southern California mantle, *J. Geophys. Res.*, *95*, 19,725–19,746, 1990.

Ichinose, G., S. Day, H. Magistrale, T. Prush, F. Vernon, and A. Edelman, Crustal thickness variations beneath the Peninsular Ranges, southern California, *Geophys. Res. Lett.*, *23*, 3095–3098, 1996.

Kikuchi, M., and H. Kanamori, *Bull. Seismol. Soc. Am.*, *72*, 491, 1982.

Ligorria, J. P., and C. J. Ammon, Iterative deconvolution and receiver-function estimation, *Bull. Seismol. Soc. Am.*, *89*, 1395–1400, 1999.

Zhao, D. P., H. Kanamori, and E. Humphreys, Simultaneous inversion of local and teleseismic data for the crust and mantle structure of southern California, *Phys. Earth Planet. Inter.*, *93*, 191–214, 1996.

Zhu, L., and H. Kanamori, Moho depth variation in southern California from teleseismic receiver functions, *J. Geophys. Res.*, *105*, 2969–2980, 2000.

Table 1: Station location, delay, crustal thickness and Vp/Vs ratio.

	Location			Station Delay[a]			Moho Ps[a,b]						
Sta.	Lat.	Long.	h	n	t	σ	n	t	σ	*Amp.*	κ	σ	th[c]
ADO	34.55	-117.43	908	172	0.1	0.2	48						
AGA	33.64	-116.40	811	296	-0.1	0.2	112	3.59	0.14	0.26	1.80	0.02	27
ALP	34.69	-118.30	754	326	-0.1	0.3	188						
BAK	35.34	-119.10	113	281	0.1	0.3	40	4.10	0.17	0.18			33
BAR	32.68	-116.67	496	675	-0.1	0.2	95	4.72	0.12	0.11			37
BBR	34.26	-116.92	2067	200	0.2	0.3	131	4.62	0.15	0.28			37
BBS	33.92	-116.98	783	131	0.1	0.2	64						
BC3	33.65	-115.45	1080	333	0.1	0.3	37	3.34	0.14	0.19			27
BCC	33.58	-117.26	393	180	-0.2	0.1	27	3.98	0.09	0.17			32
BEL	34.00	-116.00	1394	73	0.0	0.2	33	3.65	0.10	0.28	1.76	0.02	29
BFS	34.24	-117.66	1296	22	-0.2	0.2	12	4.25	0.11	0.17	1.83	0.01	31
BKR	35.27	-116.07	305	461	-0.2	0.2	117	3.28	0.13	0.17	1.71	0.01	28
BLA	34.07	-116.39	1244	244	0.0	0.3	101	4.29	0.12	0.20	1.83	0.01	31
BOR	33.27	-116.42	257	215	-0.1	0.1	101	3.06	0.16	0.17			24
BRE	33.81	-117.98	26	105	0.3	0.2	28						
BTC	33.01	-115.22	37	347	0.2	0.4	72						
BTP	34.68	-118.58	1600	434	0.0	0.3	130	4.04	0.12	0.17			32
CALB	34.14	-118.63	276	159	-0.3	0.2	79	4.42	0.21	0.19			35
CAP	33.39	-117.19	298	244	-0.3	0.1	118	4.10	0.15	0.14			33
CCC	35.52	-117.36	0	34	0.1	0.1	22	3.98	0.10	0.24	1.80	0.01	30
CHF	34.33	-118.03	1567	370	0.0	0.2	142	4.33	0.22	0.09			34
CHN	34.00	-117.68	208	230	-0.2	0.2	145						
CIA	33.40	-118.41	425	386	-0.3	0.2	102	2.80	0.14	0.14	1.64	0.02	26
CIU	33.45	-118.48	233	59	-0.2	0.2	11	2.67	0.12	0.23	1.67	0.01	24
CLC	35.82	-117.60	735	359	-0.1	0.2	169	3.60	0.10	0.21	1.78	0.02	28
CLT	34.09	-117.32	327	216	-0.2	0.2	101	4.52	0.16	0.26			36
COO	33.90	-118.22	-1	113	0.4	0.2	45						
CPP	34.06	-117.81	235	338	-0.4	0.2	51	3.77	0.28	0.17			30
CTC	33.65	-115.99	533	222	-0.2	0.2	105	3.14	0.14	0.20	1.86	0.02	22
CWC	36.44	-118.08	1553	494	0.2	0.2	78	3.91	0.10	0.20			31
DAN	34.64	-115.38	398	384	0.2	0.2	168	3.23	0.21	0.13	1.69	0.01	28
DEV	33.94	-116.58	332	401	0.0	0.3	133	4.36	0.11	0.20			35
DGR	33.65	-117.01	609	704	-0.1	0.2	159	4.30	0.13	0.17	1.79	0.01	33
DJJ	34.11	-118.45	245	378	-0.3	0.2	110	3.32	0.17	0.12	1.70	0.01	29
DLA	33.85	-118.10	15	70	0.4	0.2	18						
DPP	33.00	-116.94	470	140	-0.2	0.2	48	5.02	0.10	0.10			40

continued on next page

continued from previous page

Sta.	Lat.	Long.	h	n	t	σ	n	t	σ	*Amp.*	κ	σ	th^c
DRC	32.81	-115.45	15	305	0.6	0.3	60						
DVT	32.66	-116.10	900	41	0.2	0.2	19	3.71	0.12	0.21			29
EDW	34.88	-117.99	762	480	-0.1	0.2	93	3.67	0.09	0.16	1.74	0.01	30
EML	32.89	-116.85	172	121	-0.3	0.2	50	4.77	0.17	0.10			38
ERR	33.12	-115.82	-57	200	0.4	0.2	49	3.17	0.18	0.08			25
FIG	34.73	-119.98	1180	1	0.7	0.0	1						
FMP	33.71	-118.29	82	141	-0.2	0.2	57						
FPC	35.08	-117.58	883	406	0.1	0.1	72	3.69	0.10	0.15	1.72	0.02	31
FUR	36.47	-116.86	-24	508	0.0	0.2	137	4.26	0.15	0.13			34
GLA	33.05	-114.83	514	495	0.2	0.3	175	3.22	0.12	0.12	1.72	0.01	27
GOR	33.16	-117.23	76	315	-0.2	0.2	98	3.80	0.14	0.08			30
GPO	35.65	-117.66	735	123	-0.2	0.2	59	4.19	0.23	0.28			33
GR2	34.12	-118.30	346	392	-0.4	0.2	103	3.80	0.18	0.10	1.74	0.01	31
GRA	36.98	-117.36	652	63	0.3	0.2	39						
GSC	35.30	-116.81	954	730	0.1	0.1	137	3.61	0.16	0.15	1.73	0.01	30
HEC	34.83	-116.33	959	444	-0.0	0.2	111	3.74	0.15	0.21	1.80	0.01	28
HLL	34.18	-118.36	193	163	-0.3	0.2	69	3.80	0.29	0.17			30
ISA	35.66	-118.47	817	606	-0.2	0.4	125	4.72	0.11	0.10			37
JCS	33.09	-116.60	1259	394	0.1	0.2	115	4.14	0.32	0.07			33
JRC	35.98	-117.81	1482	486	0.2	0.2	117	4.15	0.08	0.32	1.79	0.01	32
JVA	34.37	-116.61	903	71	-0.1	0.2	36	3.73	0.06	0.23	1.74	0.01	30
LAF	33.87	-118.33	12	131	0.3	0.2	29						
LCG	34.00	-118.38	103	164	0.4	0.2	44	3.58	0.18	0.05			28
LDF	35.13	-115.18	1239	289	0.4	0.3	211	3.58	0.10	0.16	1.78	0.02	28
LFP	34.30	-118.49	367	158	0.2	0.2	48						
LGB	33.98	-118.15	36	134	0.3	0.2	41						
LGU	34.11	-119.07	381	342	-0.3	0.1	88	2.63	0.14	0.13			21
LKL	34.62	-117.82	814	522	-0.0	0.2	72	3.81	0.07	0.22	1.77	0.01	30
LLS	33.68	-117.94	6	145	0.3	0.2	38						
LRL	35.48	-117.68	1315	402	0.0	0.1	123	3.87	0.08	0.30	1.74	0.01	32
LTP	33.88	-118.18	18	36	0.5	0.2	9	3.55	0.12	0.16			28
LUG	34.37	-117.37	1140	409	0.2	0.2	137	4.44	0.20	0.25			35
MCT	34.23	-116.04	653	108	-0.2	0.2	53	3.43	0.10	0.25			27
MGE	33.82	-116.37	67	205	-0.0	0.2	63	4.12	0.21	0.26			33
MLAC	37.63	-118.84	2134	595	0.6	0.4	147						
MLS	34.00	-117.56	229	272	-0.5	0.2	83	3.97	0.13	0.14	1.75	0.01	32
MOP	34.28	-118.90	142	221	0.1	0.2	38						
MPM	36.06	-117.49	1853	321	0.2	0.2	131	3.95	0.16	0.19	1.78	0.03	31
MSJ	33.81	-116.97	500	283	0.3	0.2	83	3.69	0.37	0.04			29
MTL	34.27	-118.24	471	6	0.1	0.2	4						

continued on next page

continued from previous page

Sta.	Lat.	Long.	h	n	t	σ	n	t	σ	*Amp.*	κ	σ	th^c
MTP	35.48	-115.55	1582	470	0.1	0.2	87	3.23	0.09	0.18	1.82	0.01	24
MWC	34.22	-118.05	1696	490	-0.0	0.1	123	3.79	0.25	0.12			30
NEE	34.82	-114.60	139	466	-0.0	0.2	59						
OLI	33.95	-117.92	78	265	0.1	0.2	68						
OSI	34.61	-118.72	706	484	0.0	0.3	139	3.74	0.14	0.05			30
PAS	34.15	-118.17	257	739	-0.3	0.2	108	3.41	0.12	0.17	1.74	0.01	28
PDE	34.44	-118.58	328	239	0.2	0.2	30						
PDR	33.96	-118.44	38	16	0.3	0.1	6						
PDU	34.12	-117.64	440	309	-0.3	0.1	164	4.37	0.16	0.13	1.87	0.02	30
PFO	33.61	-116.46	1245	287	0.1	0.2	220	3.37	0.12	0.16	1.72	0.01	28
PHL	35.41	-120.55	360	449	0.1	0.2	106	3.05	0.10	0.24	1.74	0.01	25
PLC	33.82	-116.51	126	282	-0.2	0.3	150						
PLM	33.35	-116.86	1660	483	0.2	0.1	154	4.60	0.11	0.23			37
PLS	33.80	-117.61	1181	464	0.0	0.2	59	3.52	0.11	0.31	1.72	0.01	29
RCT	36.31	-119.24	107	297	-0.7	0.3	146						
RIN	34.28	-118.48	305	170	0.3	0.2	43						
RIO	34.10	-117.98	109	187	-0.1	0.2	68						
RPV	33.74	-118.40	64	675	-0.2	0.1	159	2.88	0.16	0.24	1.75	0.02	23
RRX	34.90	-117.03	680	104	0.1	0.3	66	4.02	0.16	0.26	1.75	0.02	32
RUS	34.05	-118.08	67	304	-0.1	0.2	82						
RVR	33.99	-117.38	232	375	-0.4	0.3	75	4.19	0.11	0.15	1.78	0.01	32
SAL	33.28	-115.99	12	295	0.0	0.2	85						
SBC	34.44	-119.71	61	664	0.1	0.3	53	4.26	0.11	0.15			34
SBPX	34.23	-117.23	1875	486	0.2	0.2	71	4.87	0.09	0.16			39
SCI	32.98	-118.55	219	363	-0.1	0.2	39	2.70	0.16	0.13	1.64	0.01	25
SCZ	34.00	-119.64	413	280	-0.3	0.2	86	3.27	0.18	0.11			26
SDD	33.55	-117.66	91	264	0.1	0.1	76	4.34	0.14	0.14			34
SDR	32.61	-116.93	123	69	-0.2	0.5	59	4.15	0.13	0.06			33
SES	34.44	-119.14	480	83	0.3	0.2	26	3.12	0.19	0.14			25
SHO	35.90	-116.28	373	499	-0.1	0.2	145	3.78	0.12	0.21			30
SLA	35.89	-117.28	1190	365	0.1	0.2	129	3.80	0.14	0.23	1.79	0.01	29
SMM	35.31	-120.00	631	300	0.3	0.2	85	4.33	0.19	0.15			34
SMS	34.01	-118.46	53	314	0.3	0.2	29						
SMTC	32.95	-115.72	3	24	0.4	0.2	17	3.05	0.15	0.14			24
SNCC	33.25	-119.52	227	532	-0.0	0.3	50	2.59	0.15	0.11			21
SOT	34.42	-118.45	439	462	-0.0	0.2	63	4.39	0.18	0.16			35
SPF	34.06	-118.65	464	125	-0.2	0.2	50	4.27	0.17	0.09	1.86	0.02	30
SPG	36.14	-118.81	309	300	-0.4	0.3	110	5.24	0.14	0.12	1.80	0.01	40
SRN	33.83	-117.79	211	230	0.0	0.2	72	3.84	0.25	0.15	1.81	0.02	29
SSW	33.18	-115.60	168	148	-0.1	0.3	20	3.41	0.28	0.21			27

continued on next page

continued from previous page

Sta.	Lat.	Long.	h	n	t	σ	n	t	σ	$Amp.$	κ	σ	th^c
STC	34.30	-119.19	182	190	0.6	0.3	30						
STG	33.66	-117.77	52	201	-0.2	0.1	109	3.80	0.12	0.18	1.76	0.01	30
STS	33.79	-118.20	3	125	0.3	0.2	33	3.91	0.12	0.23			31
SVD	34.11	-117.10	574	732	0.0	0.2	122	4.86	0.15	0.13			39
SWS	32.94	-115.80	134	429	-0.1	0.2	77	2.48	0.14	0.18			20
SYP	34.53	-119.98	1253	29	0.1	0.3	17	4.11	0.12	0.27			33
TA2	34.38	-117.68	2250	385	0.3	0.2	140	4.58	0.26	0.10			36
TEH	35.29	-118.42	854	67	0.1	0.3	41	4.42	0.18	0.14	1.75	0.02	36
THX	33.63	-116.16	-14	293	0.1	0.2	83						
TIN	37.05	-118.23	1164	403	0.3	0.3	147	4.63	0.14	0.26			37
TOV	34.16	-118.82	332	449	-0.2	0.1	108	3.49	0.12	0.12			28
USC	34.02	-118.29	17	589	0.3	0.2	51						
VCS	34.48	-118.12	991	446	-0.0	0.3	156	4.24	0.10	0.14	1.82	0.02	31
VES	35.84	-119.08	153	324	-0.5	0.3	68						
VTV	34.56	-117.33	812	643	-0.1	0.2	58	3.80	0.08	0.23			30
WES	32.76	-115.73	-7	77	0.2	0.2	23	2.92	0.18	0.14			23
WGR	34.51	-119.27	557	15	-0.1	0.3	4						
WLT	34.01	-117.95	98	122	-0.1	0.2	16						
WSS	34.17	-118.65	314	80	-0.1	0.2	14	4.16	0.25	0.14			33
WTT	33.95	-118.26	33	122	0.4	0.2	23						
ASBS	33.62	-116.47	1400	54	-0.0	0.2	33	3.57	0.21	0.16	1.76	0.02	28
BZN	33.49	-116.67	1301	76	0.1	0.1	32	3.99	0.17	0.16	1.78	0.01	31
CRY	33.56	-116.74	1128	66	0.0	0.1	42	4.14	0.13	0.15	1.78	0.01	32
ELKS	33.58	-116.45	1169	53	-0.1	0.1	26	3.53	0.11	0.17	1.76	0.01	28
FRD	33.49	-116.60	1164	77	0.1	0.1	52	3.70	0.11	0.24	1.72	0.01	31
GLAC	33.60	-116.48	1169	54	-0.1	0.1	34	3.53	0.11	0.20	1.75	0.01	28
KNW	33.71	-116.71	1507	75	-0.1	0.2	49	4.15	0.18	0.10	1.78	0.01	32
LVA2	33.35	-116.56	1435	70	0.2	0.1	51	3.85	0.27	0.08	1.79	0.01	29
RDM	33.63	-116.85	1365	62	-0.0	0.1	49	4.25	0.12	0.20	1.80	0.02	32
SHUM	33.63	-116.44	1195	53	-0.1	0.2	26	3.44	0.11	0.30			27
SND	33.55	-116.61	1358	78	0.2	0.1	49	4.03	0.13	0.26			32
SOL	32.84	-117.25	245	66	-0.1	0.2	36	2.92	0.18	0.16			23
WMC	33.57	-116.67	1271	77	0.1	0.1	47	3.67	0.35	0.09	1.71	0.02	31
LAC	34.39	-116.41	793	1	0.0	0.0	1	3.64	0.00	0.30	1.73	0.00	30
ALPN	32.87	-116.75	820	15	-0.2	0.1	11	4.80	0.10	0.15	1.83	0.01	35
BLSY	32.91	-116.88	530	15	-0.2	0.1	9	4.84	0.07	0.06			38
BWLW	32.84	-116.23	293	10	0.0	0.2	2	3.28	0.02	0.18			26
HONY	32.90	-116.64	888	24	-0.2	0.2	17	4.40	0.07	0.25			35
LGNA	32.84	-116.42	1727	28	0.2	0.3	10	4.11	0.10	0.11	1.82	0.01	30
MICA	32.65	-116.12	1004	25	0.1	0.1	4	3.28	0.12	0.13			26

continued on next page

continued from previous page

Sta.	Lat.	Long.	h	n	t	σ	n	t	σ	$Amp.$	κ	σ	th^c
PINE	32.83	-116.53	1071	19	-0.0	0.1	7	4.62	0.15	0.23			37

a in seconds

b for a ray-parameter of 0.06 s/km

c crustal thickness th in km